Determination of shallow shear wave velocity profiles in the Cologne/Germany area using ambient vibrations

Frank Scherbaum[1)]
Klaus-G. Hinzen[2)]
Matthias Ohrnberger[1)]

1) Institut für Geowissenschaften der Universität Potsdam, POB 601553, D-14415 Potsdam, Germany
2) Abt. für Erdbebengeologie der Universität zu Köln, Vinzenz-Palotti-Str. 26, D-51429 Bergisch Gladbach

in press Geophys. Journ. Int.,
accepted August 21, 2002

SUMMARY

We have used both single station and array methods to determine shallow shear velocity site profiles in the vicinity of the city of Cologne/Germany from ambient vibration records. Based on fk-analysis we assume that fundamental mode Rayleigh waves dominate the analysed wavefield in the frequency range of 0.7 - 2.2 Hz. According to this view a close relation exists between H/V spectral ratios and the ellipticity of the contributing Rayleigh waves. The inversion of the shape of H/V spectral ratios then provides quantitative information about the local shear wave velocity structure. However, based on tests with synthetic data believed to represent a typical situation in the Lower Rhine Embayment, dispersion curves were found to provide stronger constraints towards the absolute values of the velocity-depth model than the ellipticities. The shape of the ellipticities was found to be subject to a strong trade-off between layer thickness and average layer velocity. We have made use of this observation by combining the inversion schemes for dispersion curves and ellipticities such that the velocity-depth dependence is essentially constrained by the dispersion curves while the layer thickness is constrained by the ellipticities. In order to test this method in practice, we have used array recordings of ambient vibrations from three sites where the subsurface geology is fairly well known and geotechnical information is at least partially available. In order to keep the parameter space as simple as possible we attempted to fit only a single layer over halfspace model. However, owing to earlier studies from the region (Budny, 1984), we assume a power law depth dependence for sediment velocities. For all three sites investigated, the inversion resulted in models for which the shear wave velocity within the sediment layer both in absolute value at the surface and in depth dependence are found to be remarkably similar to the results obtained by Budny (1984) from downhole measurements. This is strong support for the interpretation of H/V spectral ratios as Rayleigh wave ellipticities. For all three sites the predicted SH wave site amplification factors at the fundamental frequency are on the order of 5-6 with a slightly smaller value south of Cologne.

Key words: Site effects, ambient vibrations, shear wave velocity profile,array measurements

1 INTRODUCTION

Seismic risk in Germany is caused by the combination of moderate seismic hazard and high vulnerability in regions of high population density and concentration of industrial facilities. The Cologne area in NW Germany is a prime example for such a situation. Adding to the shakebility in this region is the fact that the shallow subsurface structure consists mostly of soft sediments overlying much stiffer layers thus producing significant frequency dependent soil amplifications. The distribution of shear wave velocities in these sediments is the key parameter to evaluate these effects (e.g. ESG98, 1998). In this context, the analysis of ambient vibrations has gained considerable attention especially in Japan as a low cost tool to retrieve the shallow shear wave velocity structure quantitatively (Horike, 1985; Tokimatsu et al., 1992, for reviews see Kudo, 1995; Tokimatsu, 1997; Bard, 1998). These methods are now generally based on the assumption that ambient vibrations are dominated by surface waves. Single station methods as well as array methods to determine site response properties from ambient vibrations are currently in use. Among the single station methods the H/V spectral ratio is most popular. Here, ratios of spectral amplitudes of horizontal to vertical components are calculated. These spectral ratios often exhibit a distinct peak which is often empirically found to coincide with the fundamental quarter wavelength „resonance frequency“ of the transmission response (Mooney and Bolt, 1966; Lachet and Bard, 1994; Tokimatsu, 1997). However, if ambient vibrations consist mostly of surface waves, the relationship between the body wave resonance and spectral ratio peak frequencies is not straight forward. In sedimentary basins with strong impedance contrast between the soft sediments and the underlying bedrock such a relationship might not even exist (Al Yuncha and Luzon, 2000). On the other hand, in simple 1D situations spectral ratios have more to offer than resonance frequencies. In this case, average H/V spectral ratios can be assumed to measure the ellipticity of Rayleigh waves at the surface of a layered medium. Hence, the shape of H/V spectral ratios can be used to determine the shear wave velocity profile (e. g. Arai and Tokimatsu, 1998; Ishida et al., 1998, Miyakoshi et. al, 1998; Fäh et al., 2001). In contrast to single station methods, array methods make use of the dispersive properties of surface waves in layered media. Mostly vibrations measured on the vertical component are analysed in practice since they can rather safely be assumed to be dominated by Rayleigh waves. This way, shear wave velocity profiles down to several hundred meters of depths have been obtained by inversion of dispersion curves of long period surface waves (Horike, 1985; Ishida et al., 1998; Miyakoshi et. al, 1998; Yamamoto, 1998). In this paper we employ both single station and array methods to determine shallow site profiles in the Cologne area. One aspect of this paper is to determine if both techniques provide independent information towards a unique structural model (Boore and Toksöz, 1969). The main purpose, however, is to determine the degree of constraints ambient vibrations provide on the prediction of frequency dependent soil amplification in the Cologne area.

2 DATA SET

The city of Cologne, with a population close to 1 Million, is located near the southeastern end of the Lower Rhine Embayment (LRE) in NW Germany which is one of the most active seismic regions in Central Europe (Figure 1). The shallow subsurface structure consists of soft Quaternary and Tertiary sediments overlaying Devonian shales and sandstones which outcrop to the northeast and southwest. At three sites in the vicinity of the city, arrays were located near

Pulheim, Chorweiler, and Lülsdorf, respectively (Figure 2). Each array (aperture roughly 1 km) consisted of 13 elements, which were equipped with Lennartz LE5D three-component seismometers with an eigenperiod of 5 s. Due to access constraints, the arrays were operated as cross arrays following local dirt roads and/or small trails. At each array location several hours of ambient vibrations were recorded using a sampling frequency of 125 Hz. The data were subsequently visually controlled to exclude obvious transient disturbances from nearby sources (e.g., passing vehicles, walking people, and cows). For the calculation of the H/V ratios, time windows of 15 minutes were selected for each of the sensor sites. Spectra for the horizontal and vertical components were calculated from running averages of time windows with 60 s length and an overlap of 30 s. H/V spectra for the central array locations are shown as inserts on the map in Figure 2 (log/lin scale). Table 2 lists the averages and standard deviations for peak frequencies from all 13 measuring locations at each array site.
After visual quality control, dispersion curves were calculated for each array and selected time windows using a semblance based fk-analysis. In order to determine the robustness of the results, three stacking techniques for the fk-grids were applied to the same data window. In the first approach, fk-spectra were stacked for different time windows before the phase velocity was determined while in the second approach, the maxima of individual fk spectra where averaged for different time windows. In a third approach, only time windows for which the maximum coherence between all array traces falls within the range of the best 20% were analysed with the same techniques. Above 1 Hz all the techniques essentially yield the same dispersion curves while at lower frequencies the results differ. The resulting scatter was quantified as standard deviation from the sample mean and for the purpose of fitting theoretical dispersion curves used as frequency dependent weighting factors. Resulting average dispersion curves and resulting scatter (shown as error bars) are displayed in Figure 3. Stable dispersion curves could be determined for frequencies from 0.7 up to 2.2 Hz. For the following considerations we assume that the fundamental modes of Rayleigh waves dominate the analysed wavefield at least in the frequency range for which clear dispersion is observed. We searched for higher mode contributions by azimuthally stacking the fk-spectral values along circles of constant phase velocities. If several modes were present, the resulting stacks should show multiple maxima as a function of phase velocity. However, the data consistently show only one single maximum which leads us to the conclusion that fundamental mode Rayleigh waves dominate the vertical component wavefield in our data set.

3 DETERMINATION OF THE SHEAR VELOCITY PROFILE

Since the dispersion curve and the ellipticity of Rayleigh waves are both controlled by the subsurface velocity structure, in principle we can invert either of them for shear wave velocity models (e. g. Tokimatsu, 1997; Ishida et. al, 1998). This is done by minimizing the misfit between observed and theoretical dispersion curve and/or ellipticity for simplified plane layered models. Since the resulting models are not unique, however, special care has to be taken regarding the parameterization (especially since we intend to use the models to estimate local site amplifications). The common approach to search for the simplest model in terms of numbers of layers which explains the observed dispersion curve and/or ellipticity may produce models which overestimate site amplifications by introducing artificial impedance contrasts. Here, overestimation doesn't even mean conservatism in terms of site amplification since the peak frequencies might be off resulting at the end in an underestimation of site amplification at the true resonance frequencies. On the other hand, overly smooth models are also inappropriate

if the smoothness is just a consequence of lack of data resolution (e. g. frequency band limitation). This would result in an undesired underestimation of local site amplifications. Considering this dilemma, our strategy is to abandon the quest for a single best model serving all needs. Instead we attempt to find a set of good models which fit all the data adequately. To make this computationally feasible we reduce the model space to models with a single sedimentary unit over a halfspace. For this unit we allow for a power law depth dependence of the elastic parameters. For sedimentary rocks this seems to be a justifiable simplification which includes a single homogeneous layer (if the exponent approaches zero) as well as a smooth gradient model (if the unit thickness increases) as end members of a fairly simple model set. For the study area P- and S-wave velocities as well as attenuation properties were experimentally determined at 32 sites in the Lower Rhine Embayment by seismic downhole measurements (Budny, 1984). The resulting generalized relationships between dynamic soil properties and depth clearly support the assumption of power law depth dependence for compressional and shear wave velocities in the sedimentary coverage of the study area.
Another important practical aspect is the question of how to combine models obtained from dispersion curves and H/V spectral ratios. Do dispersion curves and spectral ratios of ambient vibrations provide independent information towards a unique site model? Are they sensitive to the same model features and how should the information be weighted relative to each other? Since answers to these questions may differ for different site classes we first test the performance of site structure inversion for a generic site model closely resembling the site conditions in the study area. In terms of the site characterization scheme to be adopted in the new German earthquake code (DIN4149new), the area under investigation would be characterized as subsoil class C (deep basin). Following a preparatory study for the new code by Brüstle and Stange (1999) we use their average model C with a soil type 3 as generic reference model.

3.1 Reference model for the Lower Rhine Embayment

Following the classification within the new German earthquake code, the deep basin model is characterized by a shallow (20 m) soil layer with constant geotechnical parameters. This is followed by a subsoil soft sedimentary unit with increasing shear wave velocities from 350 m/s at 20 m down to 800 m/s at a depth of 320 m where the shear velocity is assumed to jump to 1600 m/s representative of consolidated permo-mesozoic sediments. Below this depth, S wave velocities are assumed to further increase with depth down to a reference bedrock depth of 1 km. Here a first order velocity discontinuity is assumed. The halfspace velocity is 3300 m/s. The uppermost panel in Figure 4 shows (a) the shear wave velocity profile for the generic deep basin model and (b) the corresponding SH-wave transfer function (top of half space to surface) corrected for the free surface. The fundamental resonance appears close to 0.5 Hz which is in good agreement with the observed H/V peak frequencies for the study area (Table 1). To test the sensitivity of the SH wave site amplification function on model details, a set of modified models was generated (Figure 4c). For this purpose layer thicknesses and geotechnical parameters of the reference model were randomly selected from truncated normal distributions centered around the given mean values. Variablities and truncation limits were chosen to represent conceivable variations for the Lower Rhine Embayment. Figure 4d shows mean values and standard deviation of the corresponding SH-wave site amplification functions. The latter scatter more or less symmetricly around the site amplification derived from the mean model (Figure 4b) for the fundamental resonance peak while for higher frequencies this is no longer the case (Figure 4e). The individual model Figure 4a is therefore believed to be a fair representation of a typical deep basin situation regarding the fundamental resonance peak.

3.1.1 Usable frequency range

The quality of shear wave velocity profiles determined from surface waves depends crucially on the frequency range in which dispersion curve and spectral ratios (ellipticities) are suitable for the inversion. The information about the deep parts of the model is contained in the low frequency range while the shallow part is constrained by the information at high frequencies of the wavefield. The performance of an array to determine phase velocities is strongly dependent on the ratio of array aperture (a) and wavelength (λ). Decreasing a/λ, the array eventually looses its resolution to detect signal delays which are the basis for the determination of phase velocities. There is no hard rule as to where this occurs since it depends strongly on the noise conditions. Regarding the stability of H/V spectral ratios, Fäh et al. (2001) noted that for frequencies outside the range between the maximum and minimum of the ellipticity of Rayleigh waves these values become fairly sensitive to source distance effects. Consequently, for their inversion scheme they restrict the usable frequency range to the band between the maximum and the minimum of the ellipticity. Another aspect, however, is often neglected. A layered medium itself acts as a filter limiting the usable frequency range as well. To illustrate this point, we consider a single impulsive force acting obliquely to the surface of the reference model so that both Love and Rayleigh wave are generated. The (velocity proportional) amplitude spectrum for the resulting vertical and radial component seismograms (Figure 5a) demonstrate the filter effects of the model on the different wave types and components. For Love waves this effect has been theoretically discussed in detail by Tazime (1957). For practical reasons however, only vertical component records are used for the array analysis of ambient vibrations. Here, the frequency band limitation becomes especially severe at those frequencies where the amplitude of the vertical components vanishes, in other words close to the frequency of the maximum H/V spectral ratio. This is demonstrated in Figure 5b which shows the dispersion curve for the reference model color coded by the excitation strength of the vertical component of the Green's function. The low frequency limit for the determination of dispersion curves from vertical component records for a broad band source correlates very well with the lowest frequency for which we were able to determine stable dispersion curves for the study area (roughly 0.7 Hz, cf. Figure 3). Furthermore, the amplitude level of ambient vibrationsin the low frequency range is also known to be dependent on the meteorological conditions. Vertical ground motion excitation at frequencies below 0.5 Hz has been observed to be considerably increased under unstable weather conditions (Kudo, pers. comm.). This raises the question which of the factors (a) array aperture, (b) high pass filter effect of the medium, (c) source excitation strength has more influence on the depth resolution of the shear wave velocity models obtained from dispersion curve inversion. This is the topic of an ongoing study.
A similar phenomenon applies to the determination of shear wave velocity profiles from spectral ratios. Spectral ratios are distorted by contributions of unmodeled wave types (Love waves on the horizontal and body waves on all components) in the frequency ranges where there is no energy either on the horizontal or vertical component. To overcome this problem, we are currently testing an approach to separate Love and Rayleigh wave components of ambient vibrations by combined array and polarization processing based on the method of Ohrnberger (2001) but a further discussion is beyond the scope of this paper.

3.1.2 Misfit functions

To evaluate shear wave velocity models regarding their performance to explain the observed data we calculate a number of different cost functions. For the dispersion curve we use r_c defined as

$$r_c = \sqrt{\left(\sum_{i=1}^{N} \frac{(c_{obs}(f_i) - c_{theo}(f_i))^2}{\sigma_c(f_i)^2} \right) / N} \quad (1)$$

to quantify the misfit between N phase velocity values $c_{obs}(f_i)$ at observed frequencies f_i and the corresponding theoretical values $c_{theo}(f_i)$ calculated for the model under consideration. Since $\sigma_c(f_i)$ characterizes the uncertainty of the observation at frequency f_i, r_c calculates the normalized deviation of the observed dispersion curve from the model dispersion curve. A model dispersion curve which follows the upper or lower limit of the "error bars" ($c_{theo}(f_i) = c_{obs}(f_i) \pm \sigma_c(f_i)$) would result in a value of $r_c = 1$. A similar expression r_{ell} is evaluated for the misfit between the shape of observed and theoretical ellipticities. The latter are calculated including a variable fraction of Love wave energy on the horizontal component.
In order to quantify how well a model is able to predict the extreme values of spectral ratios, three additional cost functions are defined. The deviations for the extrema of the observed spectral ratios and the corresponding model ellipticities are measured by $r_{ellmax} = \sqrt{(f_{maxHV} - f_{maxEll})^2 / \sigma_{maxHV}^2}$ and $r_{ellmin} = \sqrt{(f_{minHV} - f_{minEll})^2 / \sigma_{minHV}^2}$, respectively. Finally, $r_{ellextr} = (r_{ellmax} + r_{ellmin})/2$ measures the joint misfit of the model ellipticities to explain both extreme values of the H/V spectral ratios.
Since we are dealing with relatively small model parameter sets, an exhaustive search of the model space is computationally quite feasible. This offers the advantage that the topology of the set of misfit values can be investigated in detail to check for intrinsic tradeoffs between model parameters. All the forward calculations were performed by modal summation using the code generously provided by R. B. Herrmann (Herrmann, 1996).

3.1.3 Inversion results for the Lower Rhine Embayment reference model

In order to test the resolution of the models for the study area, we tried to reconstruct the reference model (Figure 4a) from the frequency band limited synthetic dispersion curve and spectral ratios. In accordance with the observations (Fig. 3) but also based on the the considerations regarding the filter effects of a layered medium, we use 0.7 Hz as low frequency and 2.2 Hz as high frequency limit for the inversion. The corresponding model dispersion curve and ellipticity are shown in Figure 6. Figure 7 shows the resulting shear wave velocity models together with the corresponding dispersion curves and ellipticities. The left panels were obtained from the dispersion curve inversion while the right panels were obtained from the ellipticity inversion. Since the model which is used to fit the reference data (Figure 6) consists only of a single layer over halfspace (although with power law depth dependence), what we can hope to recover from the reference model at best is the shallow part. Figure 7 shows that dispersion curve and ellipticity inversion perform quite differently in this respect. From the bandlimited inversion of the dispersion curve (left panels) the velocity profile for the uppermost 200-300 m is well recovered. The depths to the first strong impedance contrast in the 20 best fitting models scatter roughly within 100 m. All the resulting model dispersion curves match the reference dispersion curve well within the frequency band used for the fit while outside this range the curves diverge drastically. This corresponds to the fact, that expectedly there is nearly no resolution for the halfspace velocity. For models obtained from the ellipticity fit (right panels) the velocity depth profile is less well recovered (uppermost right panel) even for the shallow portion. In addition to the scatter of the depths to the first strong impedance contrast, which is on the same order as for the dispersion curve fit, the velocities are also off considerably. In con-

trast to the dispersion curve, the shape of the ellipticity does obviously not constrain the absolute values of the velocity model. This can also be seen in the mismatch of the resulting dispersion curves with respect to the reference disperison curve (second panel from top). Regarding the halfspace velocities the scatter is comparable to the results obtained from the dispersion curve inversion.

3.1.4 Sensitivity of ellipticity and phase velocity regarding layer structure

Judging from the results in Figure 7, the dispersion curve seems to contain more recoverable information about the velocity structure than the shape of the ellipticities. This seems to be in conflict with the result of the study of Boore and Toksöz (1969). They concluded (based on the investigation of partial derivatives of ellipticities and phase velocities with respect to layer parameters) that both quantities were equally sensitive to layer structure. One possible explanation for our contrasting result is that we only use the shape of the ellipticity not the absolute values. The reason for this is our believe that for ambient vibrations - due to the presence of an unknown amount of Love and body waves - absolute spectral ratios will not be a very precise measure of Rayleigh wave ellipticity. For the interpretion of the shape, however, we only have to assume that these distortions are constant as a function of frequency.
In order to compare the inversion performance based on dispersion curves and ellipticities for a well controlled situation, we have tried to reconstruct the velocity model for a single gradient layer above halfspace (Figure 8). This model can be seen as a simplified version of the shallow part of the reference model for the Lower Rhine Embayment. The layer parameters were chosen following Ibs von Seht and Wohlenberg (1999) for a maximum spectral ratio at 0.5 Hz. For the inversion, only the surface shear wave velocity and the layer thickness were used as free parameters while all the other parameters were kept fixed. Again, the dispersion curve allows to reconstruct the absolute values of the velocity quite nicely while it fails to constrain the layer thickness. The models resulting from the ellipticity inversion perform less satisfactory in matching the absolute velocities as well as in matching the layer thicknesses. Considering the nonuniquess of the resulting velocity models, it is interesting to look into the distribution of the residuals (r_c and r_{ell}) as a function of the surface velocity (v_o) and layer thickness (d). This is displayed in Figure 9Figure 9Figure 9Figure 9. The absolute values of the residuals are indicated by the contour line labels. The residual plane for r_c has a clear minimum while the residual plane for r_{ell} indicates a clear tradeoff between surface velocity and layer thickness. The shape of the ellipticity is obviously insensitive to models for which $v_0/d = const$. This is equivalent to models for which the traveltime within the layer is constant. This can also be seen in Figure 10 which shows the same models as in Figure 8 only as a function of two-way traveltime (TWT) instead of depth.
We can make use of this observation by combining the dispersion curve inversion with the inversion of ellipticities. This can be done in a number of different ways, e.g. by defining and minimizing a single joint misfit function, by nested ranking of individual misfit functions, etc. The way we choose to do it here is by defining individual levels of acceptable misfits for each misfit function. Finally we keep only those models (final accepted model set) for which all the misfit functions which we want to consider jointly fall below the predefined thresholds. Below we will refer to this approach as combined inversion. In this context it is interesting to ask which misfit functions are useful in practice. Is the shape of the ellipticity really telling us something about the velocity structure or is it mainly the position of the singularities which constrains the model. There are several aspects to this question. As can be seen in Figure 7 - Figure 9 for the single layer models, the shapes of the ellipticities can be very similar for largely differing velocity models as long as the traveltime within the layer is more or less con-

stant. Since the reciprocal four-way traveltime down to the first large impedance contrast in the generic basin model correlates well with the frequency of maximum ellipticity (Figure 11), it seems sufficient to use only r_{ellmax} and possibly r_{ellmin} to constrain the traveltime within the single layer. From a practical point of view, one could also argue that due to body and Love wave contributions, it will always be hard to judge in practice to what degree H/V spectral ratios obtained from ambient vibrations will actually represent Rayleigh wave ellipticities. This is especially true for the frequency range in which the shape of the ellipticities changes most, namely close to the minimum and maximum values. One way to get around this problem is seen in the the type of preprocessing suggested by Fäh et. al. (2001). A further evaluation of this issue, however, is beyond the scope of this paper.
The result of the combined inversion for the single layer model is shown in Figure 12. It is obvious that the traveltime constraint which is caused by including r_{ellmax} as a second cost function improves the inversion considerably. The best fitting models within the final accepted model (dashed lines in Figure 12) essentially reproduce the input model. A similar improvement is obtained for the full Lower Rhine Embayment reference model as can be seen in Figure 13. Here the depth to the first strong impedance contrast at roughly 300 m is fairly well recovered, although expectedly the resolution for the deeper structure remains lacking.
Regarding the implications for hazard assessment it is interesting to ask how well the site amplification functions for the remaining model set matches those of the input model. This is displayed in Figure 13. At the fundamental resonance frequency (0.5 Hz), the inverted models underestimate the site amplification by not more than 20%.

3.2 Shear velocity profiles for the Cologne area

The results for the Lower Rhine Embayment reference model suggest that even with frequency band limited data from 1 km aperture arrays, the uppermost part of the shear velocity profiles might be recoverable by a combined inversion of dispersion curves and ellipticities. We have applied this method to the data shown in Figure 3 and Table 1. The free parameters which were inverted for are the shear wave velocity at the surface (v_0), the velocity exponent (α_s) and the layer thickness (d). Following Budny (1984), the P- wave velocity within the layer were fixed at $v_p(z) = 1470 \cdot z^{0.057}$ (v_p in [m/s] for $z > 0$ in m). For the halfspace we used $v_p = 5200$ [m/s], $v_s = 3000$ [m/s]. The densities were fixed at $\rho = 2000$ [kg/m^3] for the sediment layer and $\rho = 2700$ [kg/m^3] for the halfspace, respectively. The inversion results are displayed in Figure 14 - Figure 16.
Table 2 displays the results for those models within the final accepted model space with the lowest residuals r_{ellmax}. Considering the different techniques but also the different locations for our study and the study of Budny (1984), the results are in remarkable agreement. It should also be noted that the depth to sediment bottom at Chorweiler and Pulheim is very close which is consistent with their spatial proximity. For all three sites the predicted site amplification factors at the fundamental frequency are on the order of 5-6 with a slightly smaller value of 5 at Lülsdorf. Since a single layer (even with power law depth dependence) is a very strong simplification of the true situation, these values should be taken with a grain of salt. In order to at least partially address the question, if deeper parts of the structure which might be resolvable, we calculated an additional set of models in which we took the models given by the values in Table 2 and added a transitional layer of 100 m thickness and varying velocity between sediments and halfspace. Only for site Pulheim did we see a slight indication that including such a transitional layer would reduce the residual. This is shown in Figure 17. For site Lülsdorf and Chorweiler, the best

fitting model remained the same. The site amplification factors didn't change much neither.

4 DISCUSSION AND CONCLUSION

We have used both single station and array methods to determine shallow shear wave velocity site profiles in the Cologne area from ambient vibration records. We assume that fundamental mode Rayleigh waves dominate the analysed wavefield at least in the frequency range for which we observe dispersion. In order to keep the parameter space in the inversion simple we attempted to fit a single layer over halfspace model. However, owing to earlier studies of the region (Budny, 1984), we assume a power law depth dependence for sediment velocities. Both the dispersion curve as well as the shape of the ellipticities contain information which can be used for the inversion of the shear velocity depth model. However, dispersion curves were found to provide stronger constraints towards the absolute values of the velocity-depth model than the ellipticities. The shape of the ellipticities was found to be subject to a strong tradeoff between layer thickness and average layer velocity. We have made use of this observation by combining the inversion schemes for dispersion curves and ellipticities such that the velocity-depth dependence is essentially constrained from the dispersion curves while the layer thickness is constrained from the ellipticities. Based on the tests with synthetic data believed to be representative for the Lower Rhine Embayment, we found that we can thus reconstruct the shear wave velocity subsurface structure down to the bottom depth of the tertiary sediments at several hundreds of meters. As has been pointed out by Boore and Brown (1998), visual comparison of velocity profiles does not allow easy judgment of the corresponding site amplification effects. Therefore, we calculated the ratios of the corresponding SH wave site amplification functions with respect to the site amplification of the reference model as suggested in a slightly different form by Boore and Brown (1998). The corresponding site amplification functions only differed by approximately 20% at the fundamental resonance frequency.
The application of this method to the field observations from the Cologne area resulted in models for which the shear velocity within the sediment layer both in absolute value at the surface and in depth dependence are found to be remarkably similar with the results obtained by Budny (1984) from downhole measurements. This agreement is seen as strong support for the assumption that within the frequency band investigated the vertical component records of ambient vibrations within the study area are dominated by fundamental mode Rayleigh waves.
Although the resulting models are one dimensional, the resulting layer thicknesses may nevertheless be an important parameter. In the Los Angeles Basin for example, sediment depth has been reported to be a good proxy for three-dimensional response and basin edge effects (Field, 2000; Joyner, 2000).
We draw some practical conclusions from the results of the present study. Velocity depth models obtained from the inversion of H/V spectral ratios may suffer from the tradeoff between average velocity and layer thickness and hence may not be very reliable in terms of absolute velocity-depth values. This might be especially problematic if nonexhaustive optimization schemes (e.g. simulated annealing, genetic algorithms) are employed. On the other hand, if information on the depth dependence of shear velocity is available (e.g. from dispersion curves or shallow boreholes), peak frequencies of spectral ratios were found to constrain the layer thickness quite well. As a consequence, single station and array recordings of ambient vibrations can provide complementary information regarding a reliable determination of shallow shear velocity profiles.

5 ACKNOWLEDGMENTS

We gratefully acknowledge the continuous technical support and the organisation of the field experiments by Daniel Vollmer. We thank Georg Bissing, Sharon K. Reamer, Jürgen Mackedanz, Nebil Bayrakcioglu, Holger Gaensicke, Angela Sachse, and Rita Streich, for their help with the measurements and R. B. Herrmann for providing his software. We appreciate the thoughtful reviews and constructive comments by Kazuyoshi Kudo and Denis Jongmans. Matthias Ohrnberger was funded by EU-Grant No.EVG1-CT-2000-00026.

6 REFERENCES

Al Yuncha, Z. & Luzón, F., 2000. On the horizontal-to-vertical spectral ratio in sedimentary basins, *Bull. Seismol. Soc. Am.*, **90**, 4, 1101-1106.

Arai, H. & Tokimatsu, K., 1998. Second International Symposium on the Effects of Surface Geology on seismic motion, Yokohama, December 1-3, 1998, Balkema, 2, 637-680.

Bard, P.-Y., 1998. Microtremor measurements: a tool for site effect estimation?, State-of-the-art paper, Second International Symposium on the Effects of Surface Geology on seismic motion, Yokohama, December 1-3, 1998, Balkema, 3, 1251-1279.

Boore, D. M. & Brown, L. T., 1998. Comparing shear-wave velocity profiles from inversion of surface -wave phase velocities with downhole measurements: Systematic differences between the CXW method and downhole measurements at six USC strong-motion sites, *Seismol. Res. Letters*, **69** , 3, 222-229.

Boore, D. M. & Toksöz, M. N., 1969. Rayleigh wave particle motion and crustal structure, *Bull. Seismol. Soc. Am.*, **59**, 1, 331-346.

Brüstle, W. & Stange, S., 1999. Geologische Untergrundklassen zum Entwurf von Normspektren für DIN 4149 (neu), LRGB Baden-Württemberg, AZ: 3480.01/98-4764.

Budny, M., 1984. Seismische Bestimmung der bodendynamischen Kennwerte von oberflächennahen Schichten in Erdbebengebieten der niederrheinischen Bucht und ihre ingenieurseismologische Anwendung, Geologisches Institut der Universität zu Köln, Sonderveröffentlichungen, Nummer 57, 1984.

ESG98, 1998. Proceedings of the Second International Symposium on the Effects of Surface Geology on seismic motion, Yokohama, December 1-3, 1998, Balkema, 3 volumes.

Field, E. H., 2000. A modified ground-motion attenuation relationship for southern California that accounts for detailed site classification and a basin-depth effect, *Bull. Seismol. Soc. Am.*, **90,** S209-S221.

Fäh, D., Kind, F., & Giardini, D., 2001. A theoretical investigation of average H/V ratios, *Geophys. J. Int.*, **145**, 535-549.

Herrmann, R.B., 1996. Computer programs in seismology, Version 3.0.

Horike, M., 1985. Inversion of phase velocity of long-period microtremors to the s-wave-velocity structure down to the basement in urbanized areas, *J. Phys. Earth*, **33**, 59-96.

Ibs-von Seht, M. & Wohlenberg J., 1999. Microtremor measurements used to map thickness of soft sediments. *Bull. Seismol. Soc. Am.*, **89**, 250-259.

Ishida, H., Nozawa, T. & Niwa, M., 1998. Estimation of deep surface structure based on phase velocities and spectral ratios of long-period microtremors, Second International Symposium on the Effects of Surface Geology on seismic motion, Yokohama, December 1-3, 1998, Balkema, 2, 697-704.

Joyner, W. B., 2000. Strong motion from surface waves in deep sedimentary basins, *Bull. Seismol. Soc. Am.*, **90**, S95-S112.

Kudo, K., 1995. Practical estimates of site response, *State-of-the-Art report, Proceedings of the Fifth International Conference on Seismic Zonation, Nice*, October 1995.

Lachet, C. & Bard, P.-Y., 1994. Numerical and theoretical investigations on the possibilities and limitations of the "Nakamura's" technique, *J. Phys. Earth*, **42**, 377-397.

Myakoshi, K., Kagawa, T. & Kinoshita, S., 1998. Estimation of geological structures under the Kobe area using the array recordings of microtremors, Second International Symposium on the Effects of Surface Geology on seismic motion, Yokohama, December 1-3, 1998, Balkema, 2, 691-696.

Mooney, H. M. & Bolt, B. A., 1966. Dispersive characteristics of the first three Rayleigh modes for a single surface layer, *Bull. Seismol. Soc. Am.*, **56**, 43-67.

Ohrnberger, M, 2001. Continuous automatic classification of seismic signals of volcanic origin at Mt. Merapi, Java, Indonesia, Dissertation University of Potsdam, pp 168.

Scherbaum, F., Hinzen, K-G., Pelzing, R., Ohrnberger, M., Reamer, S.K., Sachse, A., & Streich, R., 2000. Analysis of ambient vibrations in the Lower Rhine Embayment to study local site effects, AGU fall meeting .

Tazime, K., 1957. Minimum group velocity, maximum amplitude and quarter wavelength law. Love waves in doubly stratified layers, *J. Phys. Earth*, **5**, 43-50.

Tokimatsu K., Shinzawa, K. & Kuwayama, S., 1992. Use of short-period microtremors for vs profiling, *Journ. Geotechn. Eng.*, ASCE, 118, **10**, 1544-1558.

Tokimatsu, K., 1997. Geotechnical Site characterization using surface waves, Earthquake Geotech. Eng., Ishihara (ed.), Balkema, Rotterdam, 1333-1368.

U.S. Geological Survey, 1993, Digital elevation models, data user guide 5. Reston, Virginia, 50p.

Yamamoto, H., 1998. An experiment for estimating S-wave velocity structure from phase velocities of Love and Rayleigh waves in microtremors, Second International Symposium on the Effects of Surface Geology on seismic motion, Yokohama, December 1-3, 1998, Balkema, 2, 697-704.

Figure Captions

Figure 1 Historical seismicity in the Lower Rhine Embayment since 1000 AD and instrumentally-recorded seismicity between 1950 and 1995 from the earthquake catalog of the seismological station Bensberg plotted as circles. The larger earthquakes are concentrated on the western border faults of the Rur Graben system. The dashed square outlines the location of the simplified geologic map in Figure 2. DEM based on USGS (1993).

Figure 2 Array locations and simplified geologic map of the study area.

Figure 3 Dispersion curves obtained at the three array locations. Shown from top to bottom are the dispersion curves for Chorweiler, Pulheim, and Lülsdorf, respectively. The error bars do not represent the true uncertainty but the scatter resulting from the application of different stacking techniques.

Figure 4 Reference basin model for the Lower Rhine Embayment and corresponding site amplification functions for plane SH waves. a) mean model, b) mean site amplification function, c) randomized basin models and d) corresponding site amplification functions. e) superposition of b) and d).

Figure 5 a) Excitation function (proportional to ground velocity) for the radial and vertical component of a single impulsive force acting obliquely to the surface of the reference model. b) dispersion curve for the reference model grayshaded by the vertical excitation strength.

Figure 6 Dispersion curve (a) and ellipticity (b) for the reference model shown in Figure 4a.

Figure 7 Inversion results for the Lower Rhine Embayment reference model. Shown from top to bottom are the 20 best fitting velocity-depth models followed by the corresponding dispersion curves and ellipticities, respectively. The left panels correspond to the minimization of the dispersion curve residuals (r_c) while the right panels correspond to the minimization of the ellipticity residuals (r_{ell}). The heavy solid line and the solid squares correspond to the reference model. The heavy dashed lines show the results for the inverted model with the lowest residual.

Figure 8 Inversion results for the single layer model. Shown from top to bottom are the 20 best fitting velocity-depth models followed by the corresponding dispersion curves and ellipticities, respectively. The left panels correspond to the minimization of the dispersion curve residuals (r_c) while the right panels correspond to the minimization of the ellipticity residuals (r_{ell}). The heavy solid line and the solid squares correspond to the input model. The heavy dashed lines show the results for the inverted model with the lowest residual.

Figure 9 Distribution of the residuals (r_c and r_{sr}) as a function of the surface velocity (v_o) and layer thickness (d).The upper panel corresponds to the dispersion curve residuals (r_c) while the lower panel corresponds to the ellipticity residuals (r_{ell}).

Figure 10 Inversion results for the single layer model displayed as velocity/2-way-traveltime models. The left panel corresponds to the minimization of the dispersion curve residuals (r_c) while the right panel corresponds to the minimization of the ellipticity residuals (r_{ell}). The heavy solid line corresponds to the input model. The heavy dashed line shows the results for the model with the lowest residual.

Figure 11 Frequencies of maximum (solid squares) and minimim (stars) ellipticities for the randomized basin model (Figure 4c) plotted against the reciprocal of the 4 way traveltime to the sediment/rock interface. The solid line correspond to the equation $f_{ellmax} = 1/(4 \cdot tts)$ with tts being the one-way traveltime and f_{ellmax} being

the frequency of maximum ellipticity. The dashed line correspond to the equation $f_{ellmin} = 1/(2 \cdot tts)$ with tts being the one-way traveltime and f_{ellmin} being the frequency of minimum ellipticity.

Figure 12 Combined inversion results for the single layer model based on combining r_c and r_{ellmax} as described in the text. The top row shows the remaining velocity depth models (left panel) and the velocity/2-way-traveltime models (right panel). The bottom row shows the corresponding dispersion curves (left) and ellipticities (right). The heavy solid lines correspond to the input model. The heavy long and short dashed lines correspond to the models with the lowest r_c and r_{ellmax} within the final accepted model set, respectively.

Figure 13 Combined inversion results for the Lower Rhine Embayment reference model based on combining r_c and r_{ellmax} as described in the text. The top row shows the remaining velocity depth models (left panel) and the velocity/2-way-traveltime models (right panel). The middle row shows the corresponding disperson curves (left) and ellipticities (right). The heavy solid lines correspond to the input model. The heavy long and short dashed lines correspond to the models with the lowest r_c and r_{ellmax} within the final accepted model set, respectively. The bottom row shows the ratio of site amplification functions for the remaining model set with respect to the Lower Rhine Embayment reference model shown in Figure 4b (A value of 1 corresponds to perfect match).

Figure 14 Combined inversion results for the array site Lülsdorf based on combining r_c and r_{ellmax} as described in the text. The top row shows the observed disperson curves (left) and H/V spectral ratios (right). The bottom row shows the obtained velocity depth models (left panel) and the corresponding site amplification curves (right panel). The heavy solid lines correspond to the model based on the shear velocities of Budny (1984) combined with the layer thickness estimate by Ibs von Seht and Wohlenberg (1999). The heavy long and short dashed lines correspond to the models with the lowest r_c and r_{ellmax} within the final accepted model set, respectively.

Figure 15 Combined inversion results for the array site Chorweiler based on combining r_c and r_{ellmax} as described in the text. The top row shows the observed disperson curves (left) and H/V spectral ratios (right). The bottom row shows the obtained velocity depth models (left panel) and the corresponding site amplification curves (right panel). The heavy solid lines correspond to the model based on the shear velocities of Budny (1984) combined with the layer thickness estimate by Ibs von Seht and Wohlenberg (1999). The heavy long and short dashed lines correspond to the models with the lowest r_c and r_{ellmax} within the final accepted model set, respectively.

Figure 16 Combined inversion results for the array site Pulheim based on combining r_c and r_{ellmax} as described in the text. The top row shows the observed disperson curves (left) and sH/V pectral ratios (right). The bottom row shows the obtained velocity depth models (left panel) and the corresponding site amplification curves (right panel). The heavy solid lines correspond to the model based on the shear velocities of Budny (1984) combined with the layer thickness estimate by Ibs von Seht and Wohlenberg (1999). The heavy long and short dashed lines correspond to the models with the lowest r_c and r_{ellmax} within the final accepted model set, respectively.

Figure 17 Effect of a transitional layer on the inversion results for the array site Lülsdorf. For the surface layer the model parameters were kept fixed at the values given in Table 2. An additional layer of 100 m thickness with varying shear wave velocities was included above the halfspace. The top row shows the observed dispersion curves (left) and H/V spectral ratios (right). The bottom row shows the velocity depth models (left panel) and the corresponding site amplification curves (right panel). The heavy solid lines correspond to the model based on the shear velocities of Budny (1984) combined with the layer thickness estimate following Ibs von Seht and Wohlenberg (1999). The heavy dashed lines correspond to the model with the lowest residual r_c.

Tables

Table 1 Average peak frequencies (Hz) of H/V spectra at array locations in the Cologne area. Single standard deviations from the measurements at the 13 array elements are given.

Array	**NS/V**	**EW/V**
Lülsdorf	0.38 ± 0.09	0.40 ± 0.02
Chorweiler	0.70 ± 0.02	0.71 ± 0.04
Pulheim	0.59 ± 0.02	0.59 ±0.03

Table 2 Layer parameters of the best fitting models from the final accepted model sets. Values in parenthesis refer to the v_0 and α_s values obtained by Budny (1984) and the layer thickness according to the empirical relationship by Ibs von Seht and Wohlenberg (1999).

Array	v_0 **[m/s]**	α_s	d **[m]**
Lülsdorf	170 (188)	0.24 (0.213)	280 (342)
Chorweiler	200 (188)	0.22 (0.213)	190 (157)
Pulheim	230 (188)	0.16 (0.213)	195 (195)

Figures

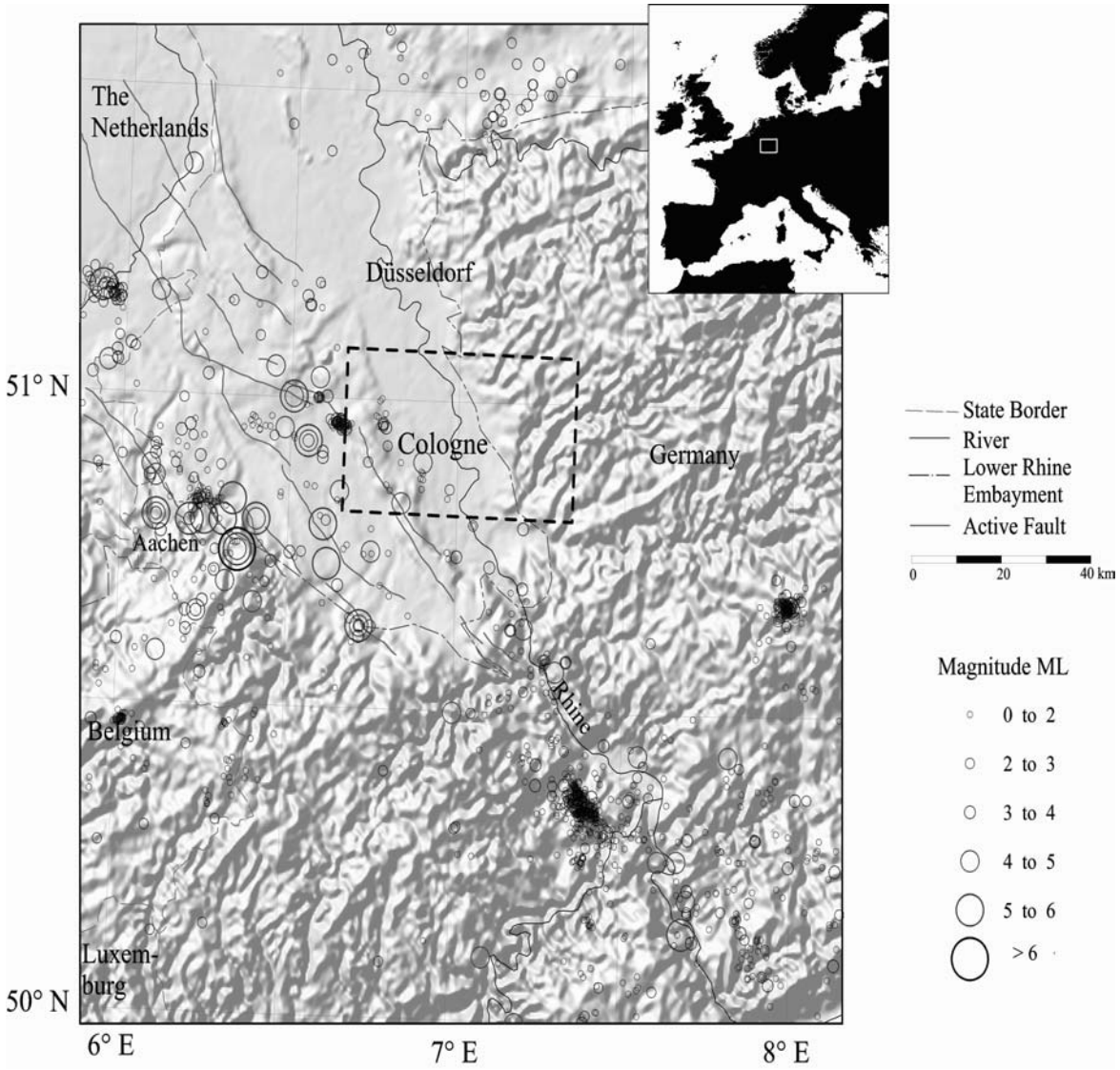

Figure 1

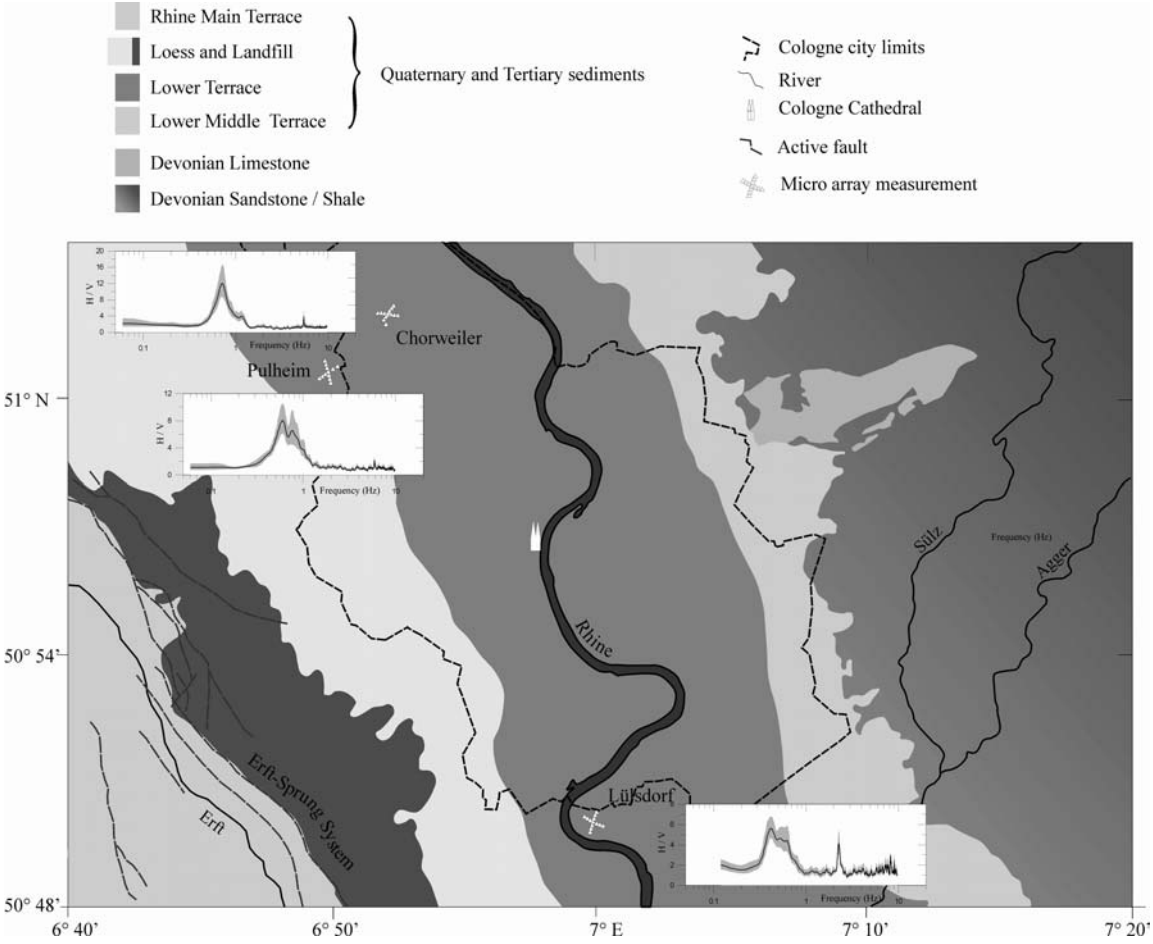

Figure 2

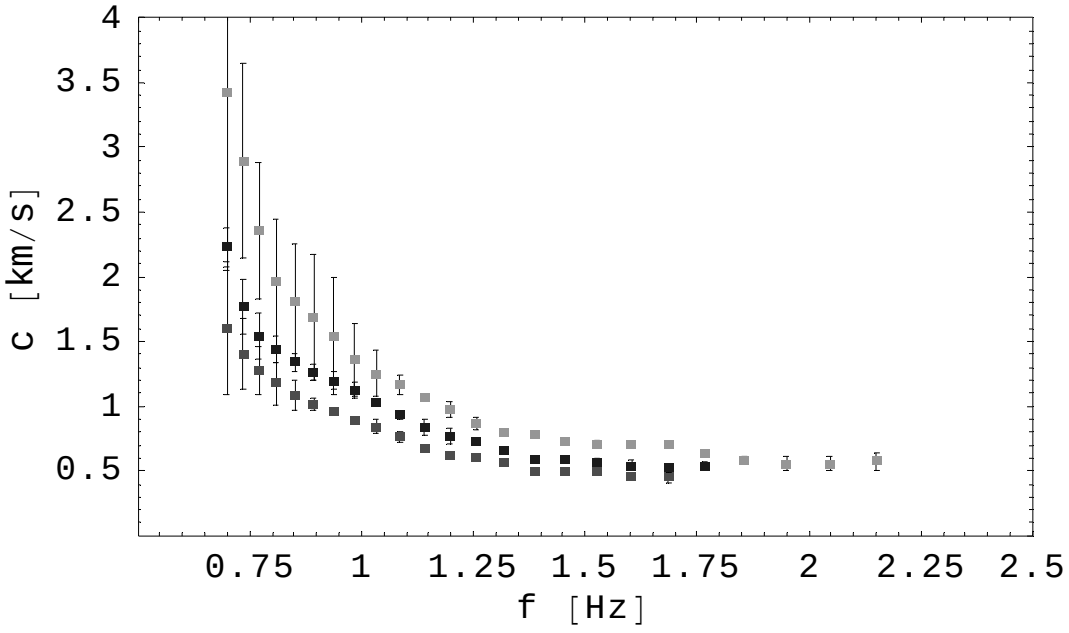

Figure 3

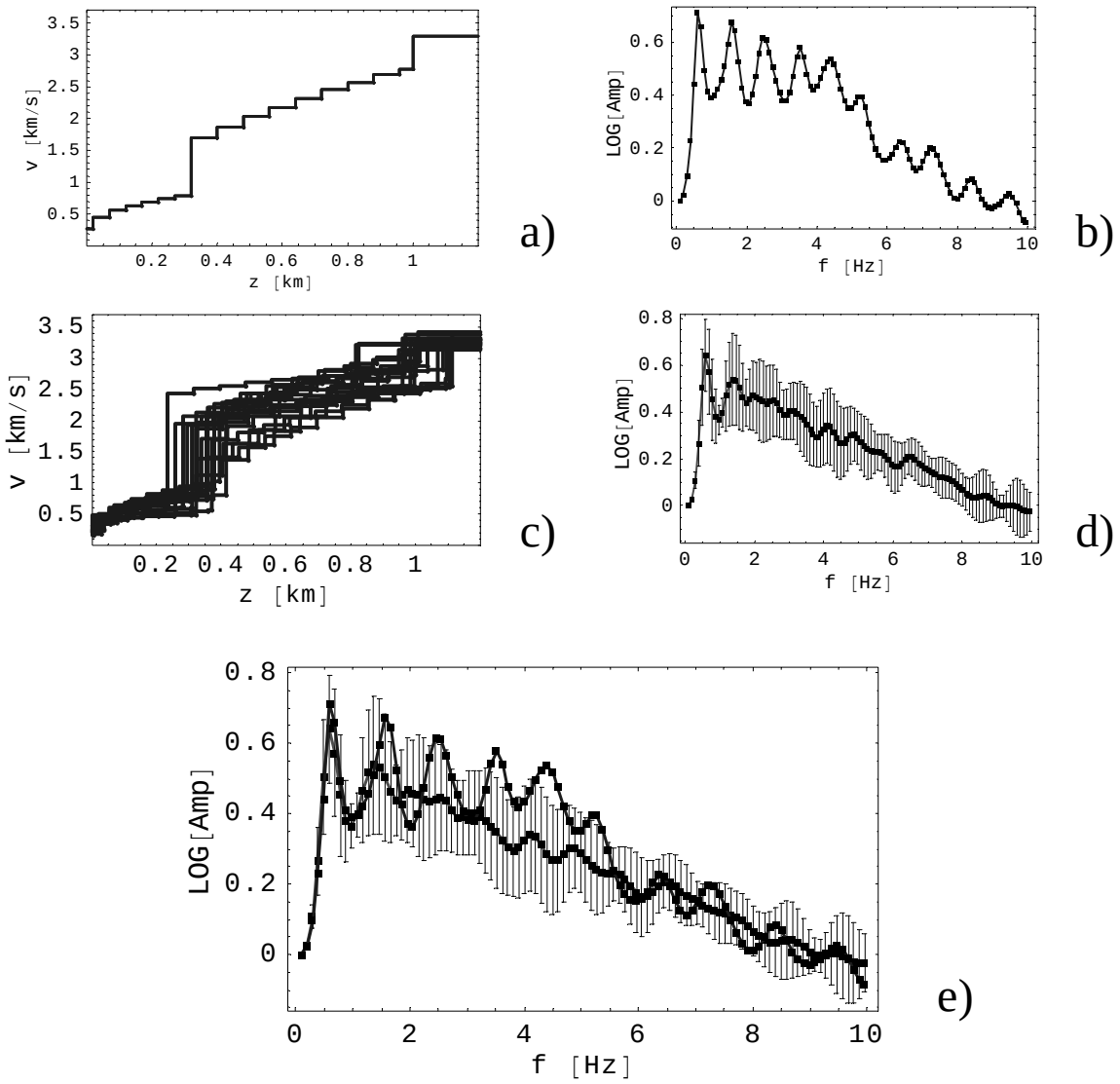

Figure 4

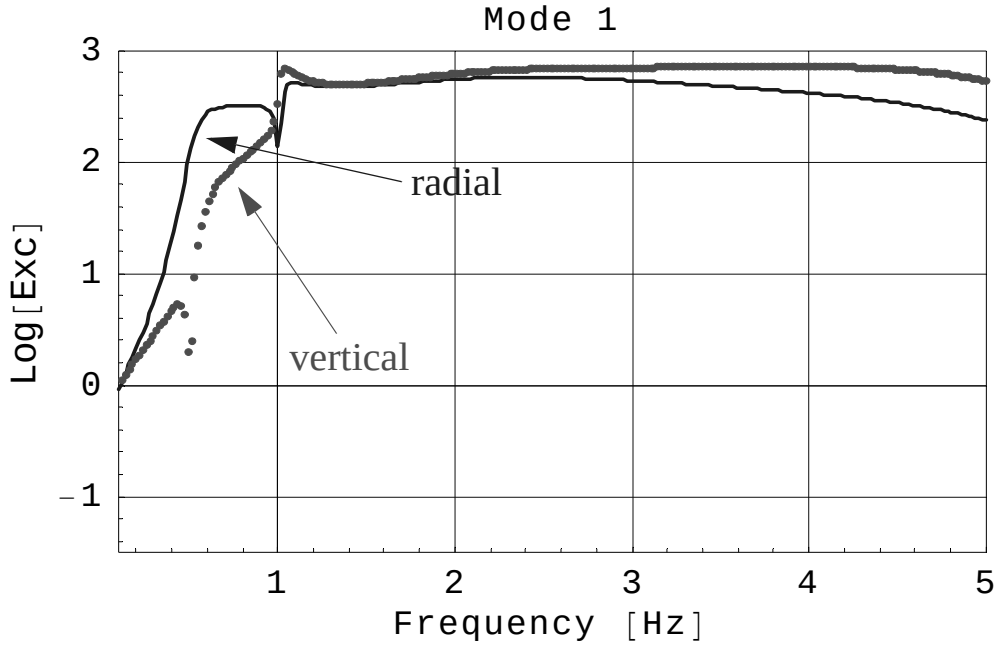
Mode 1
Log[Exc]
Frequency [Hz]
radial
vertical
3
2
1
0
−1
1
2
3
4
5

a)

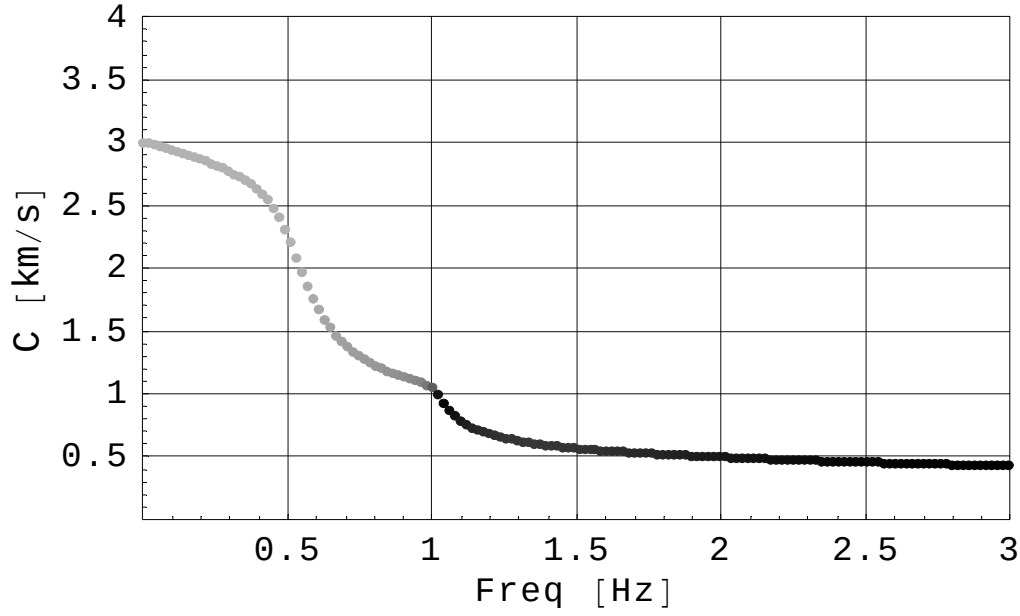
C [km/s]
Freq [Hz]
4
3.5
3
2.5
2
1.5
1
0.5
0.5
1
1.5
2
2.5
3

b)

Figure 5

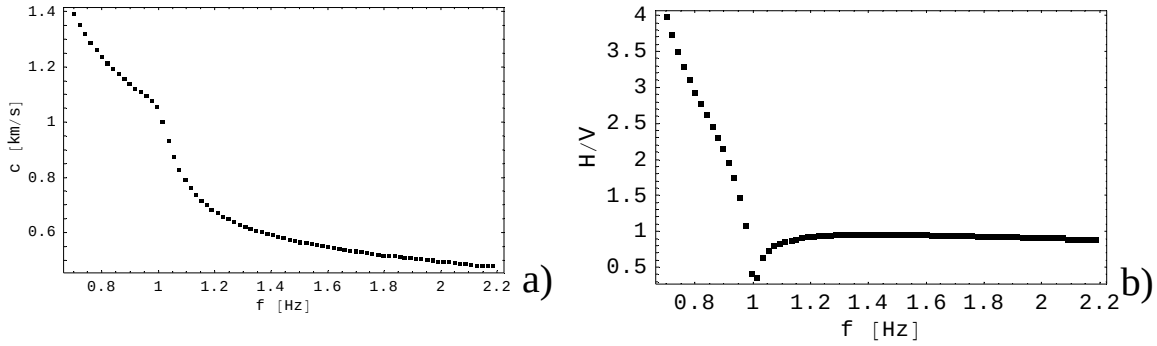

Figure 6

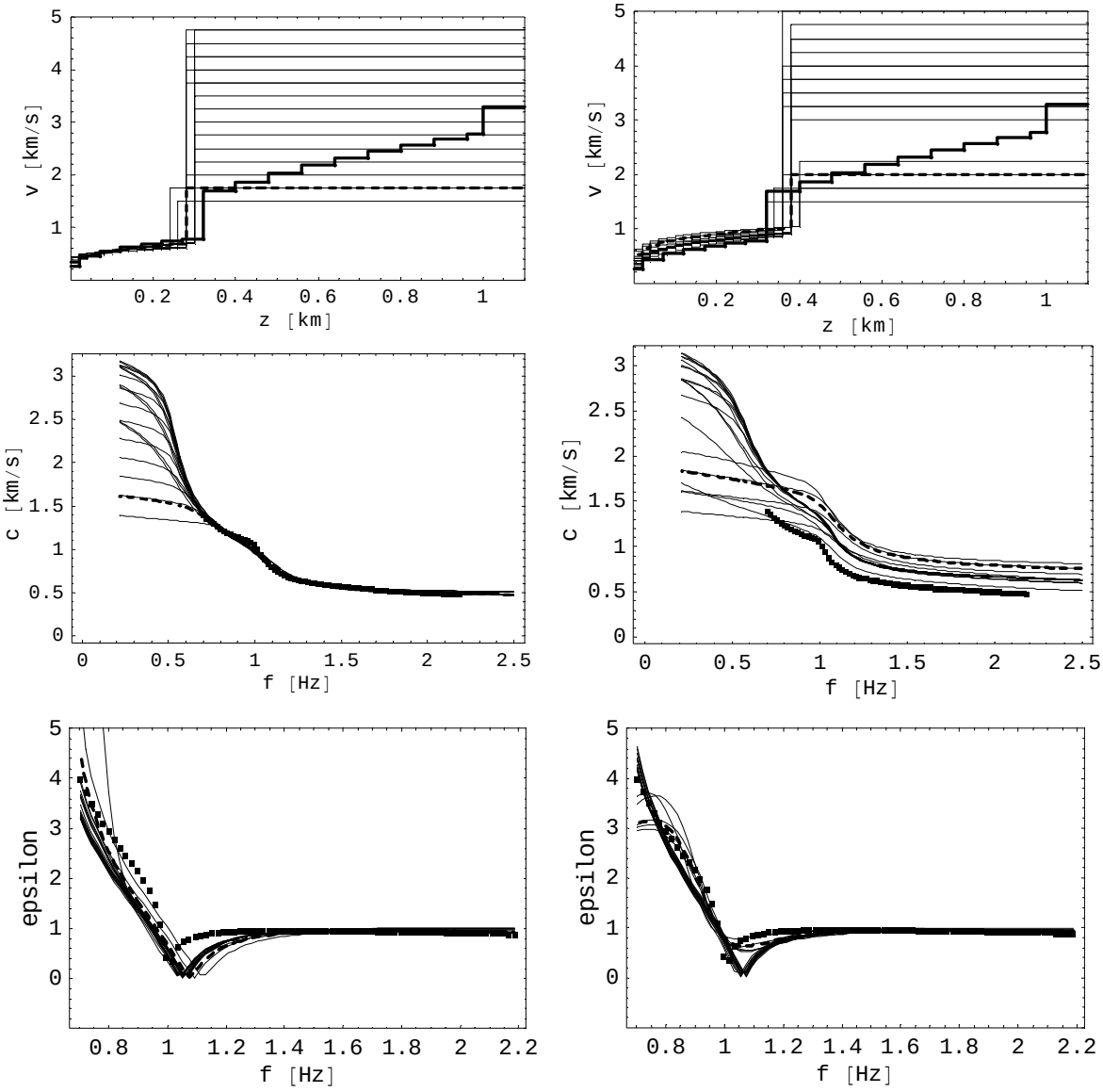

Figure 7

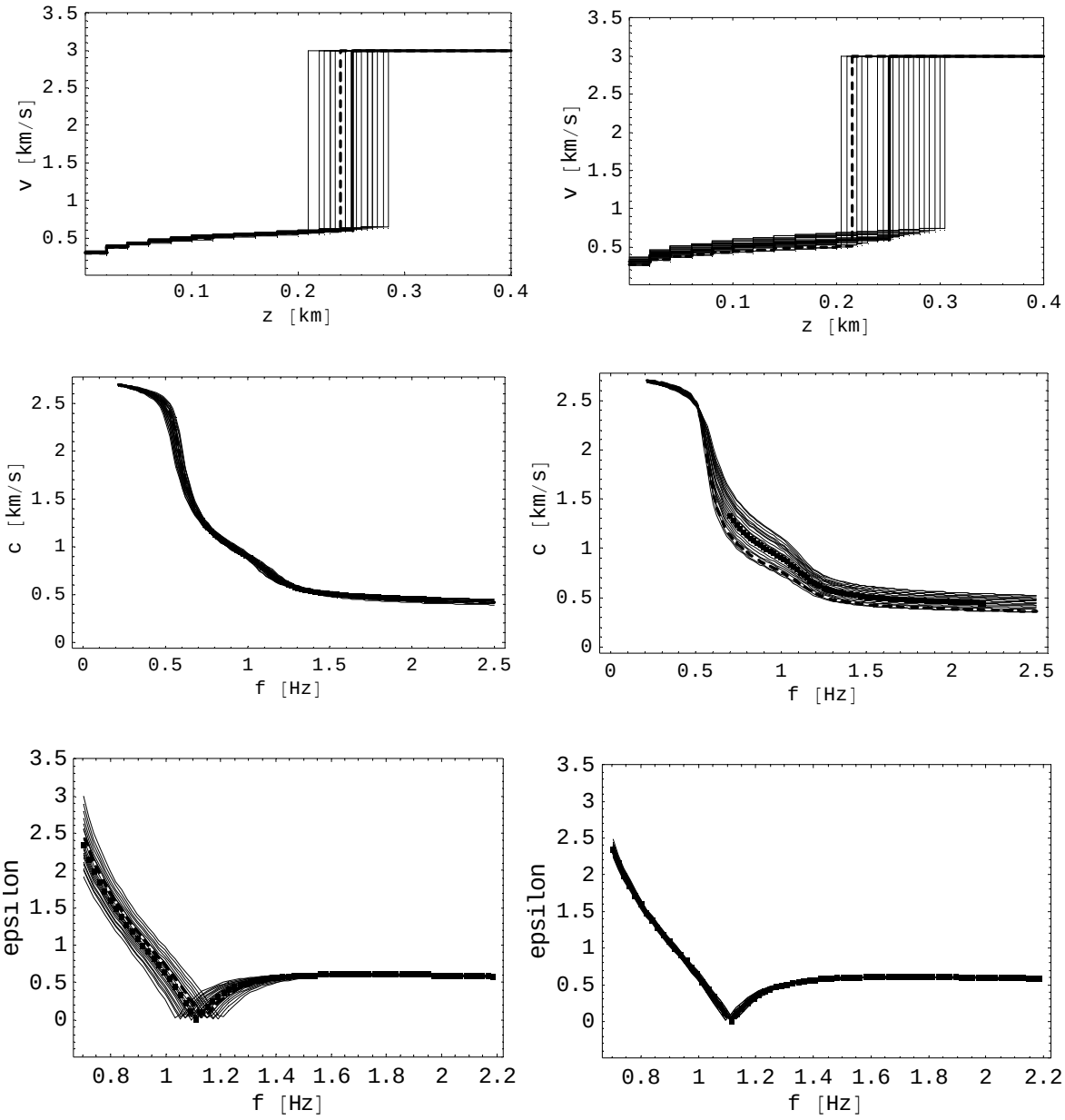

Figure 8

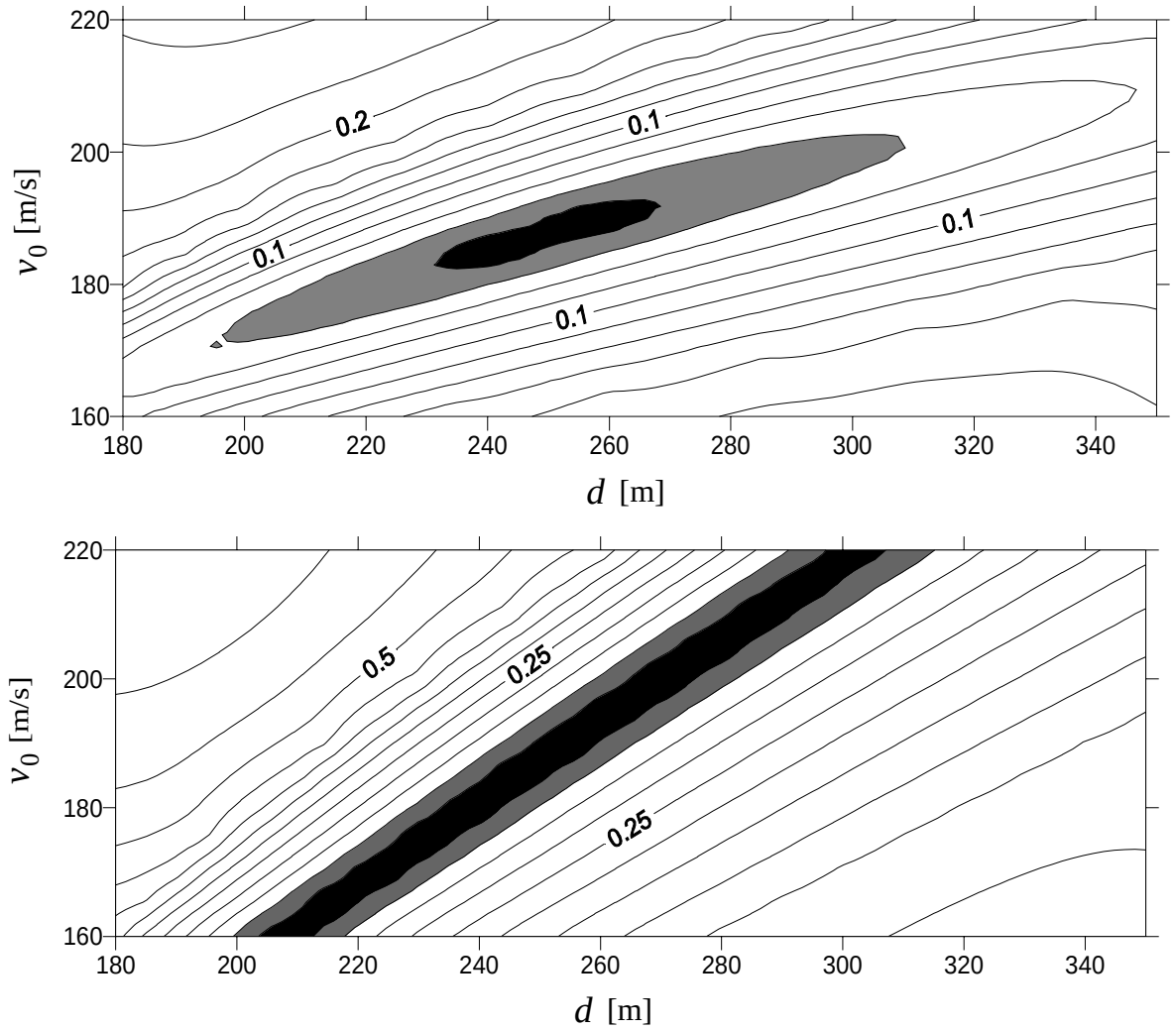

Figure 9

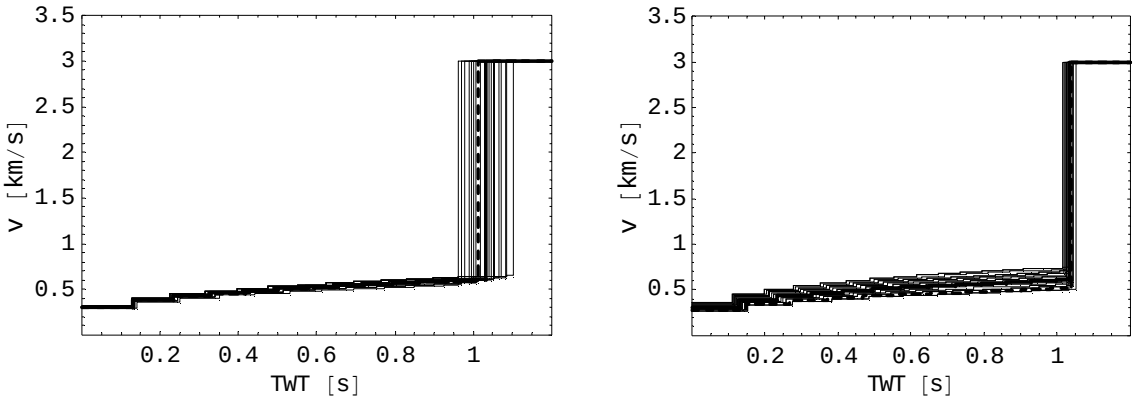

Figure 10

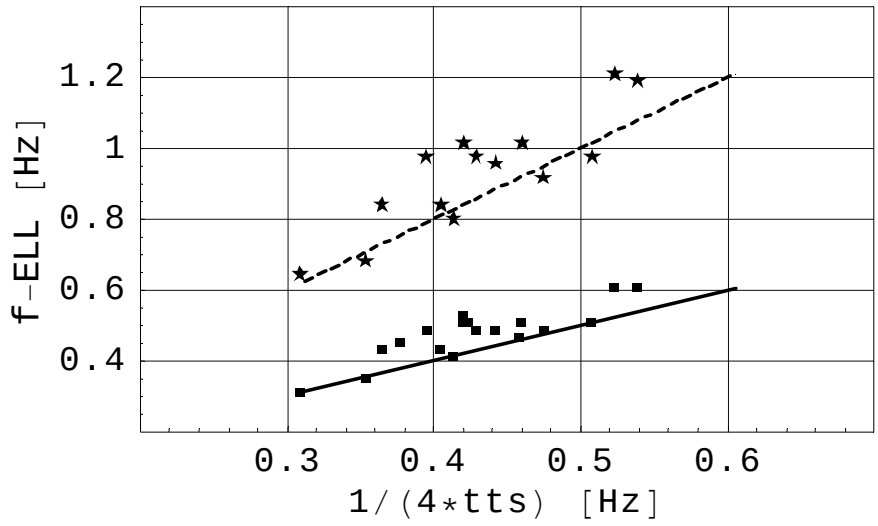

Figure 11

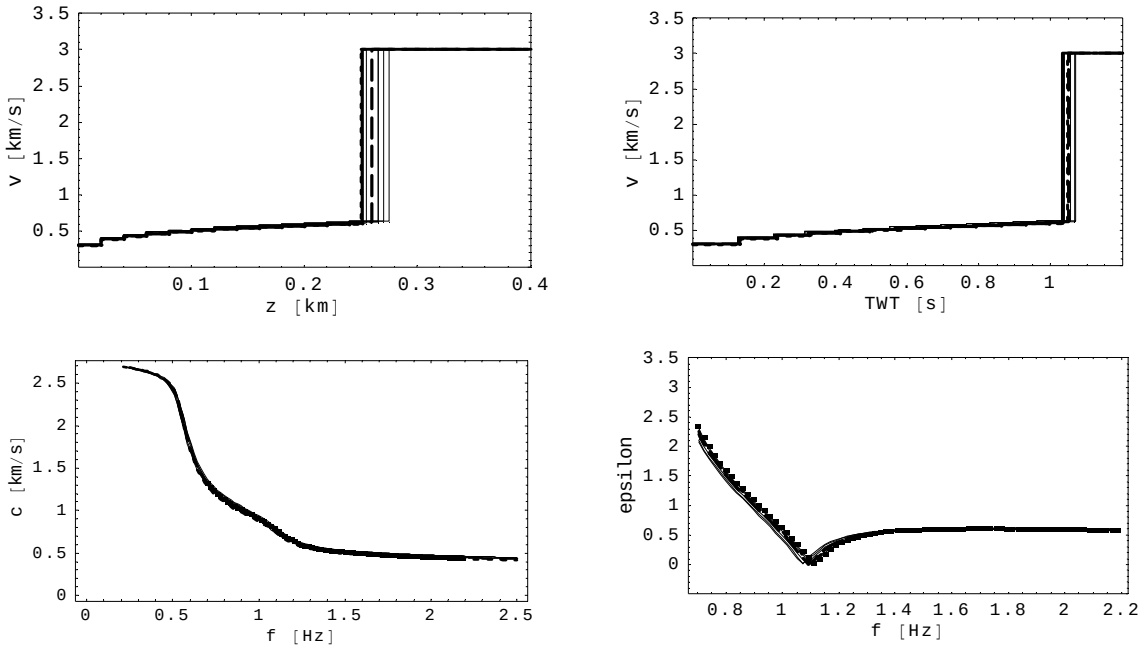

Figure 12

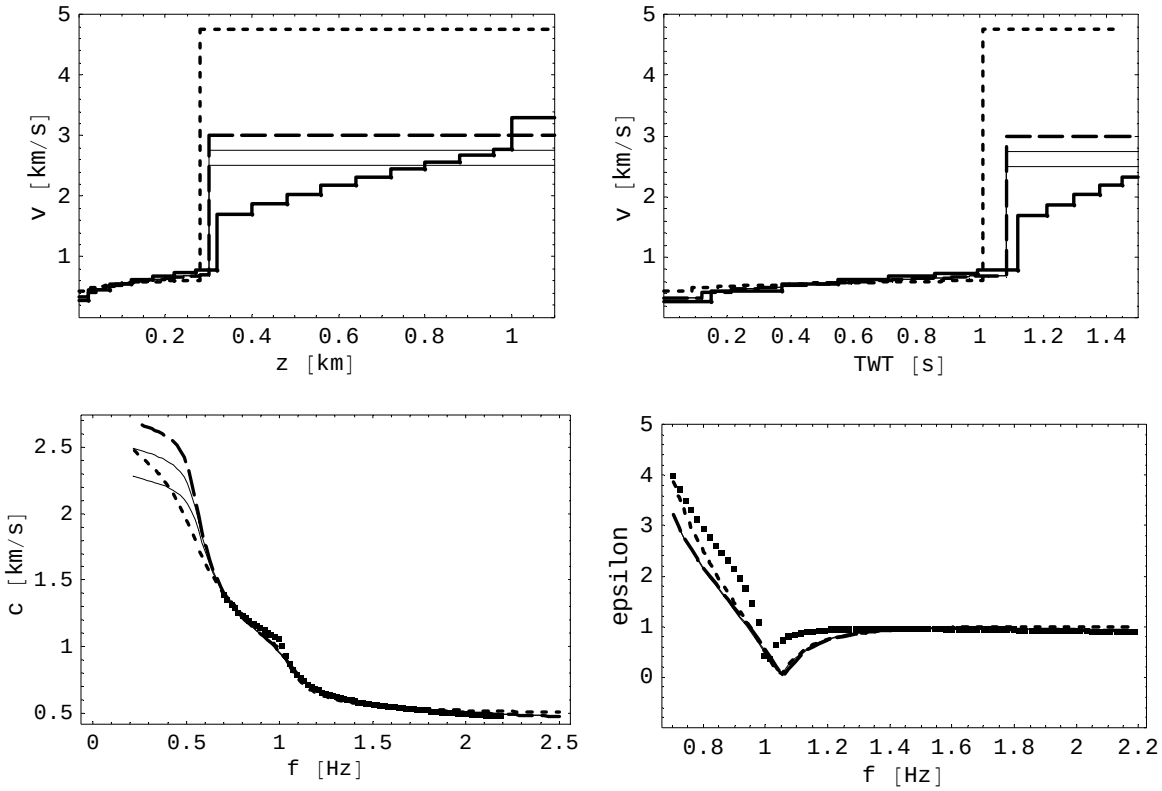

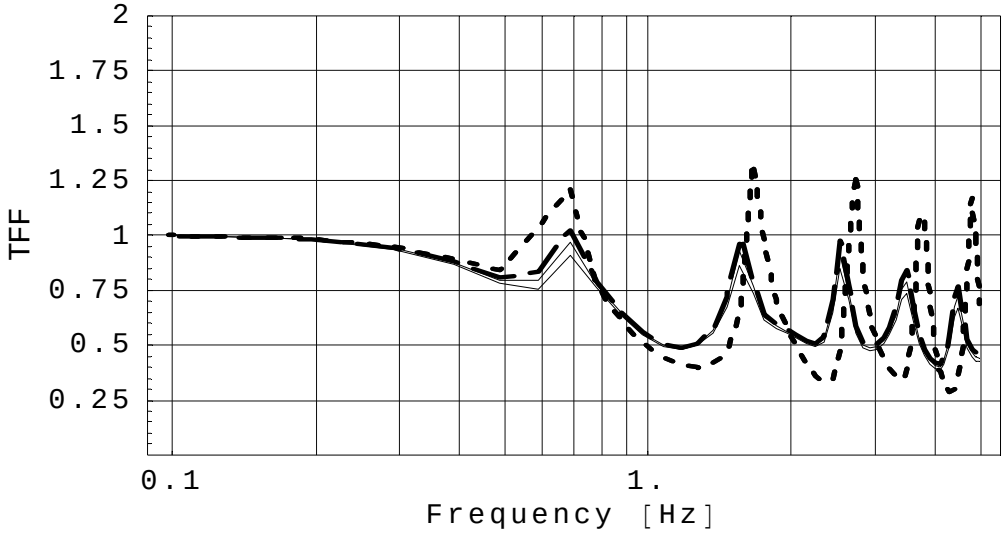

Figure 13

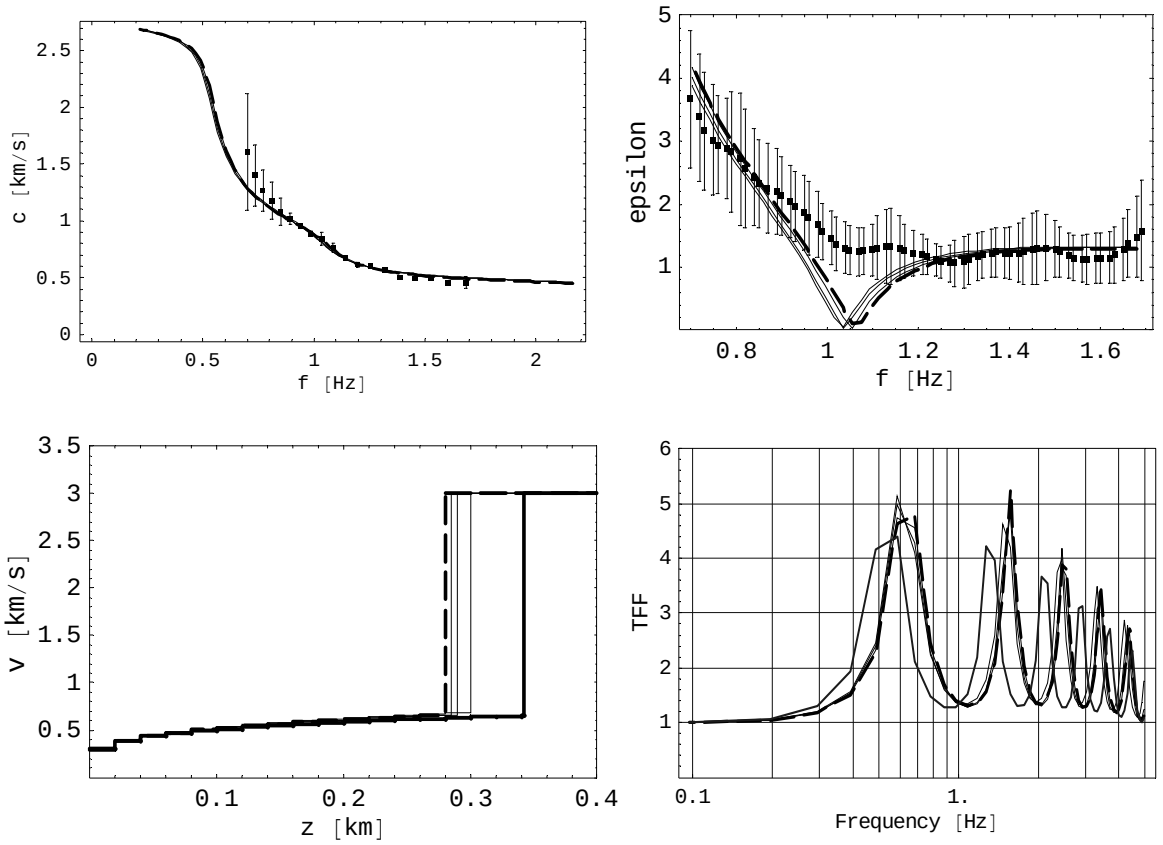

Figure 14

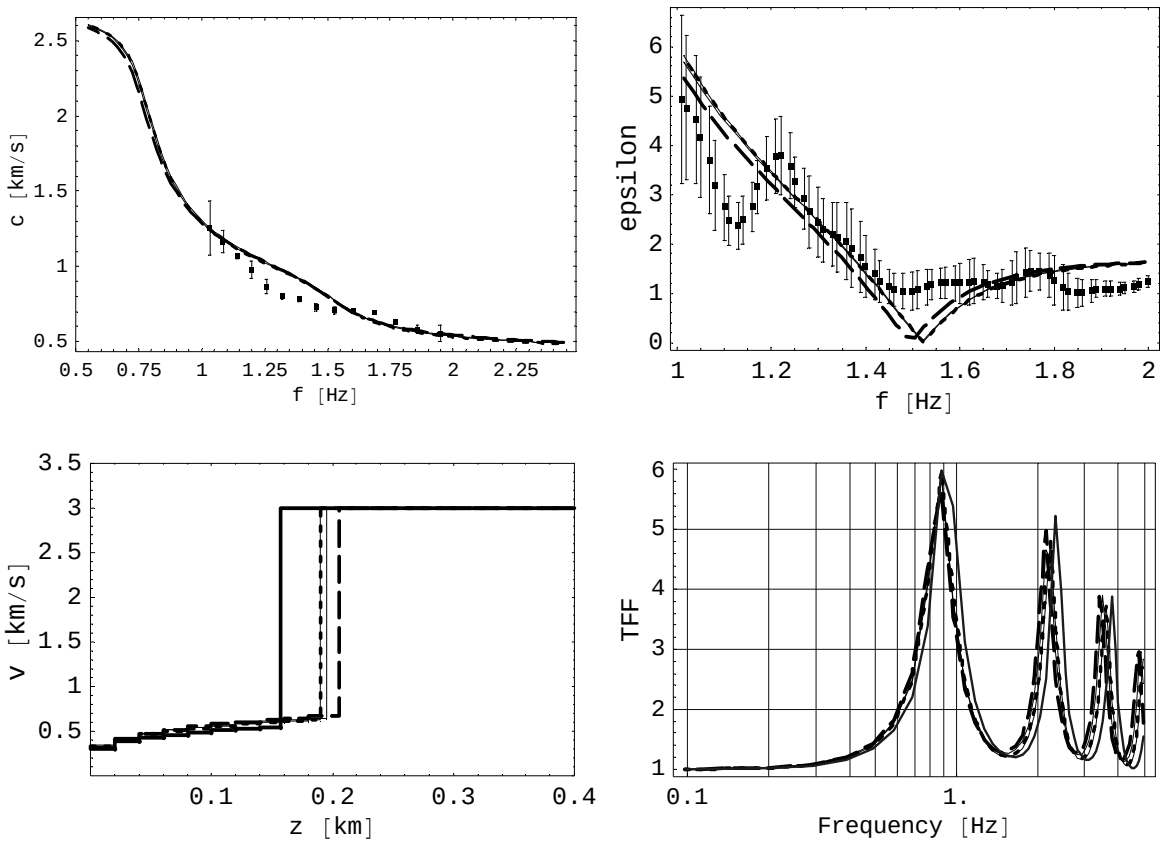

Figure 15

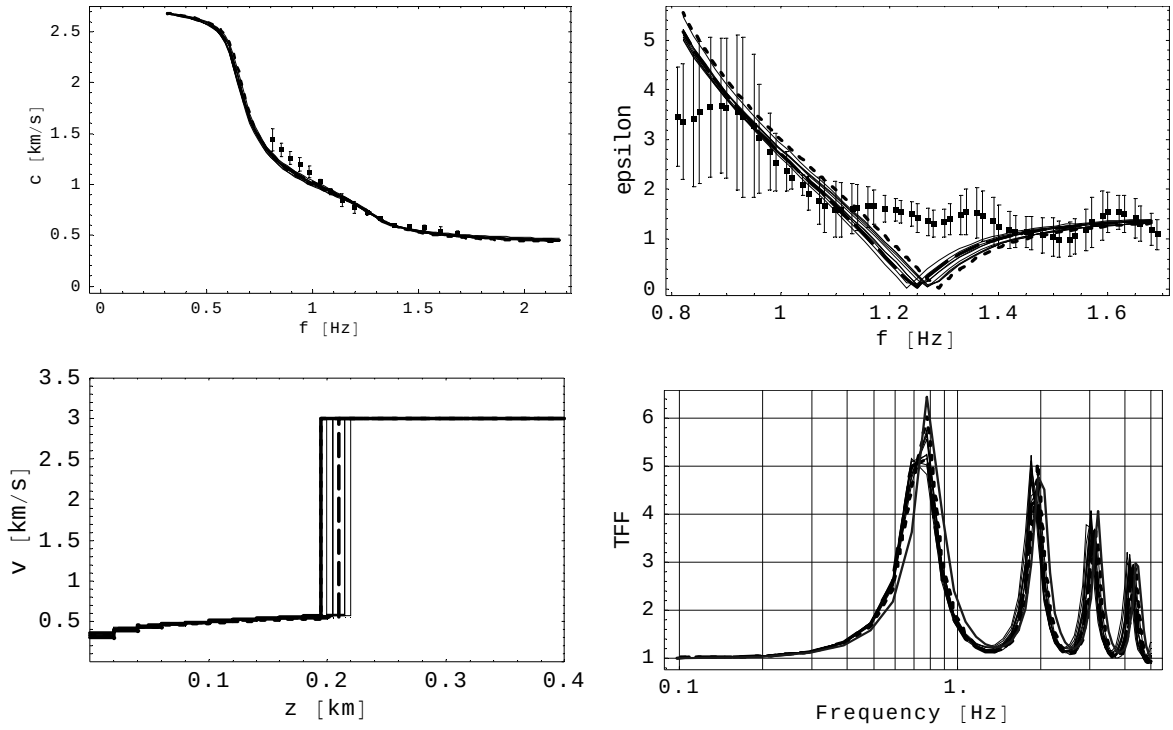

Figure 16

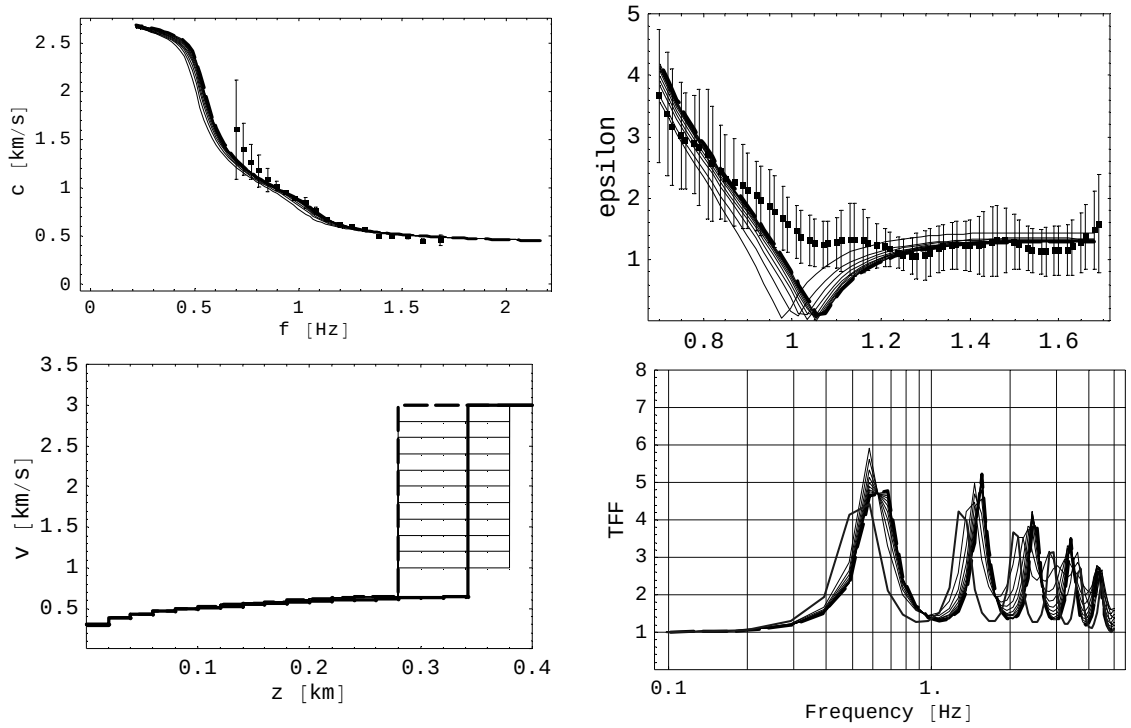

Figure 17